

On the Internal Absorption of Galaxy Clusters

John S. Arabadjis and Joel N. Bregman

University of Michigan

Dept. of Astronomy

Ann Arbor, MI 48109-1090

jsa@astro.lsa.umich.edu

jbgregman@astro.lsa.umich.edu

ABSTRACT

A study of the cores of galaxy clusters with the Einstein SSS indicated the presence of absorbing material corresponding to $10^{12} M_{\odot}$ of cold cluster gas, possibly resulting from cooling flows. Since this amount of cold gas is not confirmed by observations at other wavelengths, we examined whether this excess absorption is present in the *ROSAT* PSPC observations of 20 bright galaxy clusters. For 3/4 of the clusters, successful spectral fits were obtained with absorption due only to the Galaxy, and therefore no extra absorption is needed within the clusters, in disagreement with the results from the Einstein SSS data for some of the same clusters. For 1/4 of the clusters, none of our spectral fits was acceptable, suggesting a more complicated cluster medium than the two-temperature and cooling flow models considered here. However, even for these clusters, substantial excess absorption is not indicated.

Subject headings: galaxies: clusters – ISM: general – X-rays: ISM

1. Introduction

A central consequence of the cooling flow model for galaxy clusters is that cool gas is deposited in the central 200 kpc region at a rate that is typically $30\text{-}300 M_{\odot} \text{ y}^{-1}$ (White, Jones & Forman 1997; Allen & Fabian 1997). Although this model is consistent with a wealth of X-ray data, there has been considerable skepticism about the validity of this picture because of the difficulty in finding the end state of this cooled gas. The gas does not form stars with a normal initial mass function, so either star formation is heavily weighted to low

mass stars, the material does not form stars but remains as cooled gas, or the cooling flow model is incorrect. Consequently, there was considerable excitement when X-ray observations claimed to discover large amounts of cooled gas in galaxy clusters with approximately the masses expected from a long-lived cooling flow (White et al. 1991) (hereafter WFJMA). They used Einstein SSS data for 21 clusters, corrected for a time-dependent ice build-up, and their spectral fits yielded an absorption column which they compared to the Galactic value obtained from the large-beam Bell Labs survey (Stark et al. 1992). About half of the clusters (12/21) had X-ray absorption columns in excess of the Galactic HI column by at least 3σ , and the excess was correlated with the deduced rate of cooling gas. The mass of absorbing gas within the cluster was determined to be $3 \times 10^{11} - 10^{12} M_{\odot}$, which is approximately the amount of cooled gas that would be produced by a cooling flow over its lifetime.

The WFJMA study led to searches at other wavelengths for cold gas in cooling flow clusters, since $10^{11} - 10^{12} M_{\odot}$ of HI or H_2 would be easily detected if its properties were similar to Galactic gas. Observational searches for HI usually yielded upper limits (Jaffe 1987, 1991; Dwarkanath, van Gorkom & Owen 1994; O’Dea, Gallimore & Baum 1995), and when HI was detected, it was typically two orders of magnitude lower than the expected HI mass (Jaffe 1990; McNamara, Bregman & O’Connell 1990; Norgaard-Nielsen et al. 1993; Hansen, Jorgensen & Norgaard-Nielsen 1995). One concern was that the HI might have a velocity dispersion similar to the cluster, making it difficult to detect in narrow bandwidth studies. However, a recent wide bandwidth search for HI rules out such emission, typically at a level of $5 \times 10^9 M_{\odot}$ (O’Dea, Payne, & Kocevski 1998).

Searches for molecular hydrogen have often focused on emission or absorption from CO millimeter lines, which have led to stringent upper limits (McNamara & Jaffe 1994; O’Dea et al. 1994; Braine & Dupraz 1994; Braine et al. 1995). Recently, searches have employed the H_2 infrared lines, usually the H_2 (1-0)S(1) line, and emission has been detected in a few cases (Jaffe & Bremer 1997; Falcke et al. 1998). In their analysis of the detections, Jaffe & Bremer (1997) deduce masses that are about $10^{10} M_{\odot}$, still inadequate by two orders of magnitude to be in agreement with the X-ray observations.

Given the limits on HI and H_2 , theoretical investigations have examined whether the gas could be hidden in a form that would be difficult to detect. The work of Daines, Fabian & Thomas (1994) and of Ferland, Fabian & Johnstone (1994) indicated that the gas might be difficult to detect, with the most likely form being very cold molecular gas (near 3K). However, Voit & Donahue (1995) argue that the material is unlikely to be this cold and that the X-ray absorbing material would not have evaded detection if it were in the form of HI or H_2 . This agrees with the modeling of O’Dea et al. (1994), and the detection of the infrared

H₂ lines shows that some of the molecular gas must be warm (Jaffe & Bremer 1997). The theoretical models suggest that it would be difficult to hide cold gas from detection, although perhaps not impossible.

This apparent conflict between the WFJMA result and data at other wavebands raises the concern that there might be a problem with the SSS X-ray observations. A different group (White et al. 1994) studied four of the same clusters as WFJMA using SSS data supplemented by GINGA data as part of a study of abundance gradients in clusters. White et al. (1994) found that the amount of X-ray absorbing material depended upon various assumptions about the spectra, such as including a cooling flow in the modeling. Also, increasing the ice parameter for the SSS data would lead to a decrease in the X-ray absorbing column. In most cases, these changes could reduce but not eliminate an X-ray absorbing column in excess of the Galactic N_{HI} value. A direct conflict with the WFJMA work was presented by Tsai (1994), who used data from several instruments on the Einstein Observatory and found that toward M87, no additional X-ray absorption was required beyond the Galactic N_{HI} column.

The *ROSAT* PSPC spectra should provide a strong test of this extra absorption since it has good sensitivity across the energy band where the absorption occurs. For the clusters where the Galactic $N_{\text{HI}} \lesssim 5 \times 10^{20} \text{ cm}^{-2}$ and that have claimed excess X-ray absorption, such as M87, the Virgo Cluster, Abell 1795, Abell 2029, Abell 2142, and Abell 2199, no excess absorption is required by the PSPC data (Briel & Henry 1996; Henry & Briel 1996; Lieu et al. 1996; Sarazin, Wise & Markevitch 1998; Siddiqui, Stewart & Johnstone 1998), in direct conflict with the work of WFJMA. Also, PSPC spectra of other cooling flow clusters, such as Abell 401 and Abell 2597, fail to show excess absorption (Henry & Briel 1996; Sarazin & McNamara 1997).

It is important to note that most of these spectral fits are for a single temperature within an annulus or region. Models with cooling flows can naturally accommodate considerable internal absorbing material because these models produce soft emission (from the production of cooling gas), which can be reduced through absorption in order to agree with the observed spectrum (e.g., Wise & Sarazin (1999)). A particularly clear illustration of that is given by Siddiqui, Stewart & Johnstone (1998), who show that no excess absorption is required for either single-temperature models or cooling flow models without reheating, but that excess absorption can occur in the center for a cooling flow model with a partial covering screen. A somewhat different approach is taken by Allen & Fabian (1997) who use PSPC color maps along with a deprojection technique to fit cooling flows plus internal absorption to nearly all of their galaxy clusters. They can achieve agreement with WFJMA when they adopt a partial covering model for the absorption. The evidence suggests to us that excess absorption can be accommodated but is not required for successful spectral fits of clusters along lines

of sight where the Galactic $N_{\text{HI}} \lesssim 5 \times 10^{20} \text{ cm}^{-2}$.

The situation is different along sight lines with higher Galactic column densities, where excess columns are reported even for isothermal fits to the data. Irwin & Sarazin (1995) observed 2A0335+096, which has a Galactic $N_{\text{HI}} = 1.7 \times 10^{21} \text{ cm}^{-2}$ and found an excess of $0.6 - 1.2 \times 10^{21} \text{ cm}^{-2}$, depending upon the type of fit. A similar result is found by Allen et al. (1993), who observed Abell 478 and found an excess of $0.7 - 1.7 \times 10^{21} \text{ cm}^{-2}$ compared to the Galactic $N_{\text{HI}} = 1.4 \times 10^{21} \text{ cm}^{-2}$. An important aspect of these studies is that the excess absorption occurs both inside and outside of the cooling flow core.

Of direct relevance to this discussion is our recent study where we used the non-central regions of bright clusters to measure absorption columns for comparison with Galactic N_{HI} and N_{HII} data (Arabadjis & Bregman (1999a), hereafter AB). The motivation was that the bright isothermal parts of galaxy clusters were ideal background light sources with particularly simple spectra, so absorption columns could be determined to high accuracy. We found that for X-ray absorption columns $< 5 \times 10^{20} \text{ cm}^{-2}$, the only absorption necessary was due to Galactic N_{HI} . However, for the seven clusters with higher Galactic column densities, excess absorption was detected in every case and we attribute this excess to H_2 in the Galaxy, a result that is consistent with Copernicus H_2 studies (Savage et al. 1977). As part of our investigation, we developed software to incorporate the most recent values of the He absorption cross section, to which the results are somewhat sensitive. Here we extend the techniques that we developed to study the centers of these 20 bright clusters with the goal of determining whether excess absorption is required, and whether it is statistically different than the absorption seen in the non-central parts of galaxy clusters.

2. Method and Sample Selection

For this investigation we use the cluster sample studied in AB (Table 1). These clusters were chosen to fulfill several criteria: they must be sufficiently bright such that there were enough photons in each archived observation to constrain the spectral models; they must be well-studied so that we minimize the number of free parameters in the models; they must lie out of the plane of the Galaxy so that opacity corrections in the corresponding HI columns are minimal. The data consisted of *ROSAT* PSPC observations taken from the archives at the HEASARC. Standard packages (i.e., the PCPICOR suite in FTOOLS) were used to correct for spatial and temporal gain fluctuations in the *ROSAT* detectors (PSPC B and C; see Briel et al. (1989)). Spectra were usually taken from 3-6' and 6-9' annuli centered on the emission center of each cluster (but well outside of any possible cooling flows), over the energy range 0.14-2.4 keV (avoiding the softest channels where the calibration may be

unreliable – see Briel et al. (1989); Snowden, Turner, George & Yusaf (1995)), and modelled using both XSPEC (Arnaud 1996) and PROS (Conroy et al. 1993). Background spectra with point sources removed were generally taken from annuli with widths between 2-4' and radii between 15' and 20', and events were binned to ensure a minimum of 20 photons for each channel used in the fitting process. Each resulting background-subtracted spectrum was modelled as a single-temperature thermal plasma (model MEKAL in XSPEC; Mewe, Gronenschild & van den Oord (1985); Mewe, Lemen & van den Oord (1986); Arnaud & Rothenflug (1996); Kaastra (1992)) at a fixed temperature and redshift (White, Jones & Forman 1997) and metallicity (0.3 solar) and with variable Galactic absorption and spectral normalization. As mentioned above, we have replaced the neutral helium cross sections of Bałucińska-Church & McCammon (1992) in XSPEC with the more recent calculations of Yan, Sadeghpour & Dalgarno (1998), and set the helium abundance $\text{He}/\text{H} = 0.10$ (see discussion in AB and in Arabadjis & Bregman (1999b)).

In the present study our goal is to determine if we can model the emission from a 3' disk at the emission center using the same Galactic absorption column as that derived from X-ray fits to the outer regions, rendering an absorption component local to the cluster unnecessary. For each cluster we try to fit a single-component thermal plasma at the same temperature, redshift, and metallicity (T , z , and Z) as the models of AB. This leaves only one free parameter, the spectral normalization.

Many galaxy clusters appear to exhibit a spatial metallicity gradient, especially those containing cooling flows (Fabian & Pringle 1977; Ponman et al. 1990; Koyama, Takano & Tawara 1991; Matsumoto et al. 1996; Ezawa et al. 1997; Hwang et al. 1997). Roughly speaking, the metallicity ranges from 0.3-0.5 in the outer regions to approximately solar at the cooling flow center (Edge & Stewart 1991; Fukazawa et al. 1994; Mushotzky et al. 1996; Hwang et al. 1997; Allen & Fabian 1997). Allowing the metallicity to vary in our models often produces implausible values, however, with $Z \sim 4 - 20$. This seems to be the result of a competition between metallicity and absorption to reproduce the sharpness of the spectral peak at 1 keV; i.e., the feature can be sharpened either by increasing the Galactic column or increasing the metallicity. For our models the simplest solution is to use 0.3 for the thermal plasma metallicity, and if the fit obtained is unacceptable (e.g., one in which the reduced chi-squared χ_r^2 of the fit exceeds 1.26 for 187 degrees of freedom, indicating a probability of less than 1%), we increase it to 0.5. For the cooling flows we adopt $Z = 1$. Our choice of metallicity does not have a large effect upon our derived absorption columns, although it should be noted that the effect is somewhat greater for the resulting mass deposition rates, reducing them by 10-20% when Z is increased to 0.5 from 0.3.

If increasing the metallicity to 0.5 fails to improve the fit, we add a second thermal

plasma at the same redshift and metallicity. This adds two free parameters, the temperature and normalization of the second emission component. If this results in an unacceptable fit, we allow the absorption column to vary. The models used for each cluster are shown in Table 2.

In order to facilitate a comparison with the WFJMA results we also run cooling flow models (i.e., a thermal plasma plus emission from a cooling flow) for each cluster. We use the model of Mushotzsky & Szymkowiak (1998) (i.e. the CFLOW routine in XSPEC) for the cooling flow component, as did WFJMA. The addition of the cooling flow adds a number of free parameters: the temperature range T_{lo} and T_{up} of the emitting material, the slope α of the power law emissivity function, and the cooling flow mass deposition rate \dot{M} , as well as the redshift and metallicity. In these models we set T_{up} to the temperature of the thermal plasma component (as was done in the WFJMA study), leaving T_{lo} a free parameter. We note that T_{lo} could have been set to an arbitrarily low value (where the gas no longer contributes to emission in the soft band), but allowing it to vary produced slightly better fits in a few instances. In any case, the differences in the fits produced by the two methods are quite small. We assume an emission measure that is proportional to the inverse of the cooling time at the local flow temperature, corresponding to $\alpha = 0$. The cooling rate \dot{M} is left as a free parameter.

For each cluster we fit several cooling flow models which differ in their approach to the absorption. The first model holds the intervening column constant, at the Galactic value of AB. The second model allows the column to vary. It could be argued that any additional absorption seen in this model is not truly “local”, however, since it is manifest only as an increase in the Galactic column. Therefore we run a third model wherein the Galactic column is fixed (at a value determined in AB) and a separate, redshifted absorber covers only the central cooling flow. It should be noted, however, that such an approach does not allow for the expected small-scale structure in the Galactic interstellar medium ($\sim 7\%$ on these scales; AB), nor is the poor spectral resolution of *ROSAT* data capable of distinguishing between absorbers with differing (low) redshifts.

3. Results

Most of the clusters in our sample do not require an extra absorption component to be modelled successfully. Model fits for each cluster are shown in Table 2. Of the 20 clusters in the sample, 12 can be fit with a one- or two-component model with the intervening column set to the Galactic N_x value, and thus require no extra absorption component. Figure 1 shows an acceptable model spectrum, convolved with the PSPC instrument profile,

for Coma (Abell 1656), a cluster in the direction of low Galactic absorption. The model used here consists of one emission component at a temperature of 8.0 keV, with a Galactic column set to $0.60 \times 10^{20} \text{ cm}^{-2}$, a value determined from fits to the X-ray emission more than $6'$ minutes from the emission center. (A nearby region was determined by AB to have a column of $0.78 \times 10^{20} \text{ cm}^{-2}$. Both of these values deviate from the 21 cm column of Hartmann & Burton (1997) by more than the expected 5-7% – see AB for a discussion.) Figure 2 shows the fit for Abell 2657, which lies in a direction of relatively large Galactic column ($N_x = 1.13 \times 10^{21} \text{ cm}^{-2}$). This model also uses a single emission component ($T = 3.4 \text{ keV}$), with the column set to the value derived for an annulus 3-6'.

For the 8 clusters that cannot be fit adequately using N_x from AB, we allow the Galactic column to vary in order to ascertain whether extra absorption is required. *In no case do we achieve an acceptable fit* (i.e., $\chi_r^2 < 1.26$) *by allowing the column density to deviate from the value obtained using the outer parts of each cluster.* In three of these clusters, however, the fits are only marginally unacceptable. Abell 85 ($\chi_r^2 = 1.307$; Figure 3) requires absorption about 6% higher than the Galactic N_x value at a significance of about 1.5σ , rather weak evidence for an absorption component local to the cluster. The best fit for Abell 496 ($\chi_r^2 = 1.273$; Figure 4) requires a Galactic column which is about 8% *lower* than the nominal N_x value at about the 2.6σ level. The brighter of the two emission peaks in Abell 2256 can be fit equally well using either the Galactic column from AB or by allowing N_x to vary. In the latter case the resulting column is *lower*, but by less than 3% (less than 1σ significance).

The difference between the N_x fit in the center and in the outer parts of each cluster is expected from normal fluctuations of Galactic N_H on these angular scales, which are typically at the 5-7% level (Crovisier & Dickey 1983; Schlegel, Finkbeiner & Davis 1998; Arabadjis & Bregman 1999a). Alternatively, they may be the result of small calibration errors in the PSPC response matrices (Prieto, Hasinger & Snowden 1994). Neither Abell 85 nor Abell 496 shows a systematic fluctuation in its residuals, which would undermine confidence in the choice of models used, but the nominal uncertainty in each channel is perhaps too small, artificially inflating the χ^2 value of the fit. Such calibration errors probably dominate the χ^2 of the best-fit model for Abell 1795. The fit is unacceptable ($\chi_r^2 = 3.85$), but the residual pattern in Figure 5 demonstrates the effect of a probable gain offset below 0.5 keV (Prieto, Hasinger & Snowden 1994) coupled with small statistical errors derived from the large number of counts (6×10^5). The cooling flow model fit of A1795 is of equally poor quality, but the resulting excess column is closer to the Galactic value (+19% for the cooling flow versus +29% for the two-thermal component model).

Two-component model fits to the remaining 5 clusters are poor, but if they are physically significant they show the same behavior as the rest of the sample. Allowing each of their

Galactic columns to vary does reduce the χ^2 of the fit, yielding a model with a higher column, although the significance of this is difficult to ascertain due to the poor significance of the resulting model. If we assume that these fits are physically significant, the columns exceed their Galactic values by $\leq 38\%$ (48% for the cooling flow models), which is typically an order of magnitude smaller than the excesses found by WFJMA (see Table 3). For example, clusters displaying absorption above the Galactic value in both studies (Abell 85, 1795, 2029, and 2199), but otherwise do not seem to be unusual in N_{H} , show an excess that is 40 times greater in WFJMA than in the present work.

The models of WJFMA all contain cooling flows, so for completeness we ran cooling flow models with variable absorption (both Galactic and proximal to the cooling flow) for the entire sample. For those models which contain only a Galactic absorption component (as a free parameter), in no case was a substantial excess absorption required to model the emission. We cannot rule out the presence of a significant quantity of cool gas at the center of cooling flows, but we stress that a significant excess absorption is not a *required* feature of these spectra. Of the internally absorbed cooling flow clusters common to both WFJMA and this study, only one quarter show significant excess absorption. The fact that any show significant absorption is not surprising, since absorption can be invoked to obscure any amount of cooling flow emission; that only a quarter actually display this behavior suggests that excess internal absorption is probably not a ubiquitous feature of these systems.

It is difficult to compare these results with those of Allen & Fabian (1997) since the methods differ significantly; however, one point is worth mentioning. The “color profile” approach that they adopted used data from 0.4 keV through 2 keV. In low Galactic column clusters most of the absorption is manifest from 0.2 to 0.4 keV, where our technique is quite sensitive. For example, they compute an excess N_{H} of almost 600% for A2029, whereas our two-component model is only 11% larger than the Galactic value (and lower still for our externally absorbed cooling flow model; see Table 3).

Figures 6 and 7 show a direct comparison between between our cooling flow models of 2A0335+096 and A0085, respectively, and those of the WFJMA study. The first spectrum shown in each figure with its residuals is the application of the WFJMA model to the *ROSAT* data. Each of the model’s two absorption components (the Galactic column and an absorber in proximity to the cooling flow), plasma temperature, and cooling flow mass deposition rate are taken from WFJMA, while the plasma normalization is left as a free parameter. The emission and absorption physics used in WJFMA, Raymond & Smith (1977) and Morrison & McCammon (1983), respectively, is also used here. The second spectrum plotted in each figure is the single absorption component (i.e. a variable Galactic column) cooling flow model of this study. In both cases our fit is significantly better than WFJMA

(2A0335: $\chi_r^2 = 1.11$ vs. 2.05; A0085: $\chi_r^2 = 1.15$ vs. 8.70). In the case of 2A0335, we find an excess column approximately half that of WFJMA. For A0085, however, it is more than an order of magnitude lower.

4. Summary and Conclusions

We have examined the centers of 20 X-ray bright galaxy clusters for evidence of internal absorption by cool gas. 12 of the 20 clusters can be adequately fit by a one- or two-component model using the Galactic column density determined through X-ray absorption to the outer regions of each cluster. None of the best-fit models of the 8 remaining clusters becomes an acceptable fit by allowing the absorption to vary, although three of them are borderline cases (i.e., their reduced chi-squared values are close to the cut-off of 1.26). Their columns each deviate from the Galactic absorption to the outer parts of the clusters by 3-8%, much less than the large deviations found by WFJMA, and two of these three have a *lower* value. This is consistent with emission contrasts due to small-scale structure in the Galactic interstellar medium, therefore no change in N_x beyond those expected are seen. The remaining cluster centers are not fit successfully by either the one-component or two-component models used here, and although allowing their columns to vary does reduce their χ^2 values, they never reach acceptable levels. However, if we assume that these best fits yield valid information about N_H , the resulting column density increases are only 11-38%, more than an order of magnitude below those seen by WFJMA. At least 3/4 of this sample require no absorption beyond that expected from the Galaxy. Cooling flow models wherein the sole (Galactic) absorption component is left as a free parameter show excess absorption at least an order of magnitude lower than those seen in WJFMA.

We suggest that the discrepancy between our work and that of WFJMA is probably due to the Einstein SSS calibration. The WFJMA results depend upon the values chosen for the SSS ice buildup parameters, and although they used the best available values, there could be significant uncertainties. The time-dependent thickness of the ice buildup varied with position on the solid state detector, producing an extra absorption component (equivalent to absorption of between 10^{20} and 10^{21} cm^{-2}) that is significantly larger than many of the columns being measured. The standard model for the behavior of the ice buildup attempts to correct for the extra absorption, and is valid to a low energy cut-off near the oxygen edge at 0.5 keV (Madejski et al. 1991). Unfortunately, low and intermediate Galactic columns ($N_G \leq 5 \times 10^{20}$ cm^{-2}) are most readily measured in the 0.14-0.5 keV band (AB), limiting confidence in these measurements. Although the data no longer *require* extra N_x , it may be possible to accommodate extra absorbing material in certain models (Siddiqui, Stewart &

Johnstone 1998; Wise & Sarazin 1999).

We would like to acknowledge financial support from NASA grant NAG5-3247. We would also like to thank J. Irwin and M. Sulkanen for many useful discussions.

REFERENCES

- Allen, S.W., & Fabian, A.C. 1997, MNRAS, 286, 583
- Allen, S.W., Fabian, A. C.; Johnstone, White, D.A., Daines, S.J., Edge, A.C., & Stewart, G.C. 1993, MNRAS, 262, 901
- Arabadjis, J.S., & Bregman, J.N. 1999a, ApJ, 510, 806 [AB]
- Arabadjis, J.S., & Bregman, J.N. 1999b, ApJ, 514, 607
- Arnaud, K.A. 1996, *Astronomical Data Analysis Software and Systems V*, George H. Jacoby & Jeannette Barnes, eds., ASP Conf. Ser., 101, 17
- Arnaud, M., & Rothenflug, M. 1995, A&AS, 60, 425
- Bałucińska-Church, M., & McCammon, D. 1992, ApJ, 400, 699
- Braine, J., & Dupraz, C. 1994, A&A, 283, 407
- Braine, J., Wyrowski, F., Radford, S.J.E., Henkel, C., & Lesch, H. 1995, A&A, 293, 315
- Briel, U.G., Burkert, W., & Pfeffermann, E. 1989, *X-ray Calibration of the ROSAT Position-sensitive Proportional Counter: the Energy Calibration*, in *EUV, X-Ray, and Gamma-Ray Instrumentation for Astronomy and Atomic Physics*, Charles J. Hailey & Oswald H. Siegmund, Eds., *Proc. SPIE*, **1159**, 263.
- Briel, U.G., & Henry, J.P. 1996, ApJ, 472, 131
- Conroy, M.A., DePonte, J., Moran, J.F., Orszak, J.S., Roberts, W.P., & Schmidt, D. 1993, *Astronomical Data Analysis Software and Systems II*, R. J. Hanisch, R. J. V. Brissenden, & Jeannette Barnes, eds., ASP Conf. Ser., 52, 238
- Crovisier, J., & Dickey, M. 1983, A&A, 122, 282
- Daines, S.J., Fabian, A.C., & Thomas, P.A. 1994, MNRAS, 268, 1060
- Dwarakanath, K.S., van Gorkom, J.H., & Owen, F.N. 1994, ApJ, 432, 469
- Edge, A.C., & Stewart, G. 1991, MNRAS, 252, 414
- Ezawa, H., Fukazawa, Y., Makishima, K., Ohashi, T., Takahara, F., Xu, H., & Yamasaki, N.Y. 1997, ApJL, 490, L33
- Fabian, A.C., & Pringle, J.E. 1977, MNRAS, 181, 5

- Falcke, H., Rieke, M.J., Rieke, G.H., Simpson, C., & Wilson, A.S. 1998, *ApJ*, 494, L155
- Ferland, G.J., Fabian, A.C., & Johnstone, R.M. 1994, *MNRAS*, 266, 399
- Fukazawa, Y., Ohashi, T., Fabian, A.C., Canizares, C.R., Ikebe, Y., Makishima, K., Mushotzky, R. F., & Yamashita, K. 1994, *PASJ*, 46, L55
- Hansen, L., Jorgensen, H.E., & Norgaard-Nielsen, H.U. 1995, *A&A*, 297, 13
- Hartmann, D., & Burton, W.B. 1997, *Atlas of Galactic Neutral Hydrogen*, Cambridge University Press.
- Henry, J.P., & Briel, U.G. 1996, *ApJ*, 472, 137
- Hwang, U., Mushotzky, R.F., Loewenstein, M., Markert, T.H., Fukazawa, Y., & Matsumoto, H. 1997, *ApJ*, 476, 560
- Irwin, J.A., & Sarazin, C.L. 1995, *ApJ*, 455, 497
- Jaffe, W. 1987, *A&A*, 171, 378
- Jaffe, W. 1990, *A&A*, 240, 254
- Jaffe, W. 1991, *A&A*, 250, 67
- Jaffe, W., & Bremer, M.N. 1997, *MNRAS*, 284, L1
- Kaastra, J.S. 1992, *An X-Ray Spectral Code for Optically Thin Plasmas*, Internal SRON-Leiden Report, version 2.0.
- Koyama, K., Takano, S., & Tawara, Y. 1991, *Nature*, 350, 135
- Lieu, R., Mittaz, J.P.D., Bowyer, S., Lockman, F.J., Hwang, C-y., & Schmitt, J.H.M.M. 1996, *ApJ*, 458, L5
- Madejski, G.M., Mushotzky, R.F., Weaver, K.A., Arnaud, K.A., & Urry, C.M. 1991, *ApJ*, 370, 198
- Matsumoto, H., Koyama, K., Awaki, H., Tomida, H., Tsuru, T., Mushotzky, R., & Hatsukade, I. 1996, *PASJ*, 48, 201
- Mewe, R., Gronenschild, E.H.B.M., & van den Oord, G.H.J. 1985, *A&AS*, 62, 197
- Mewe, R., Lemen, J.R., & van den Oord, G.H.J. 1986, *A&AS*, 65, 511

- McNamara, B.R., & Jaffe, W. 1994, *A&A*, 281, 673
- McNamara, B.R., Bregman, J.N., & O’Connell, R.W. 1990, *ApJ*, 360, 20
- Morrison, R., & McCammon, D. 1983, *ApJ*, 270, 119
- Mushotzky, R., Loewenstein, M., Arnaud, K.A., Tamura, T., Fukazawa, Y., Matsushita, K., Kikuchi, K., & Hatsukade, I. 1996, *ApJ*, 466, 686
- Mushotzky, R.F., & Szymkowiak, A.E. 1988, in *Cooling Flows in Clusters and Galaxies*, Proceedings of the NATO Advanced Research Workshop, ed. A.C. Fabian, Kluwer Academic Publishers.
- Norgaard-Nielsen, H.U., Goudfrooij, P., Jorgensen, H.E., & Hansen, L. 1993, *A&A*, 279, 61
- O’Dea, C.P., Baum, S.A., Maloney, P.R., Tacconi, L.J., & Sparks, W.B. 1994, *ApJ*, 422, 467
- O’Dea, C.P., Gallimore, J.F., & Baum, S.A. 1995, *AJ*, 109, 1669
- O’Dea, C.P., Payne, H.E., & Kocevski, D. 1998, *AJ*, 116, 623
- Ponman, T.J., Bertram, D., Church, M.J., Eyles, C.J., & Watt, M.P. 1990, *Nature*, 347, 450
- Prieto, M.A., Hasinger, G., & Snowden, S. 1994, *ROSAT PSPC Calibration: Gain Variations*, MPE Calibration Memo TN-ROS-MPE-ZA00/032.
- Raymond, J.C., & Smith, B.W. 1977, *ApJS*, 35, 419
- Sarazin, C.L., and McNamara, B.R. 1997, *ApJ*, 480, 203
- Sarazin, C.L., Wise, M.W., & Markevitch, M.L. 1998, *ApJ*, 498, 606
- Savage, B.D., Bohlin, R.C., Drake, J.F., & Budich, W. 1977, *ApJ*, 216, 291
- Schlegel, D.J., Finkbeiner, D.P., & Davis, M. 1998, *ApJ*, 500, 525
- Siddiqui, H., Stewart, G.C., & Johnstone, R.M. 1998, *A&A*, 334, 71
- Snowden, S.L., Turner T.J., George J.M., & Yusaf R. 1995, *OGIP Calibration Memo CAL/ROS/95-003*.
- Stark, A.A., Gammie, C.F., Wilson, R.W., Bally, J., Linke, R.A., Heiles, C., & Hurwitz, M. 1992, *ApJS*, 79, 77
- Tsai, J.C. 1994, *ApJ*, 423, 143

Voit, G.M., & Donahue, M. 1995, ApJ, 452, 164

White, D.A., Fabian, A.C., Johnstone, R.M., Mushotzky, R.F., & Arnaud, K.A. 1991, MNRAS, 252, 72 [WFJMA]

White, D.A., Jones, C., & Forman, W. 1997, MNRAS, 292, 419

White, R.E., III, Day, C.S.R., Hatsukade, I., & Hughes, J.P. 1994, ApJ, 433, 583

Wise, M.W., & Sarazin, C.L. 1999, astro-ph/9903119.

Yan, M., Sadeghpour, H.R., & Dalgarno, A. 1998, ApJ, 496, 1044

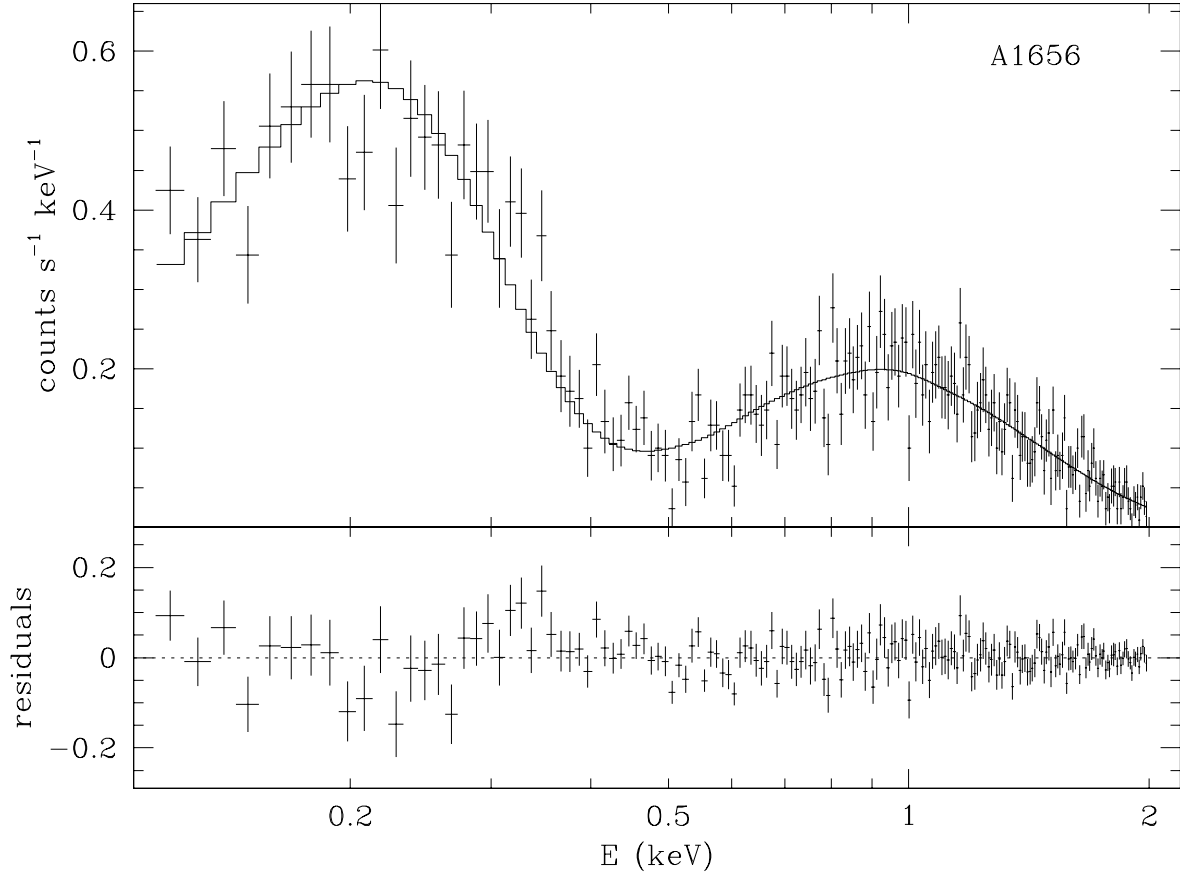


Fig. 1.— Model spectrum of Coma (Abell 1656). The model used is a single thermal plasma emission component with intervening absorption set to the Galactic N_{x} value from AB. The fit is acceptable, with $\chi_r^2 = 1.136$.

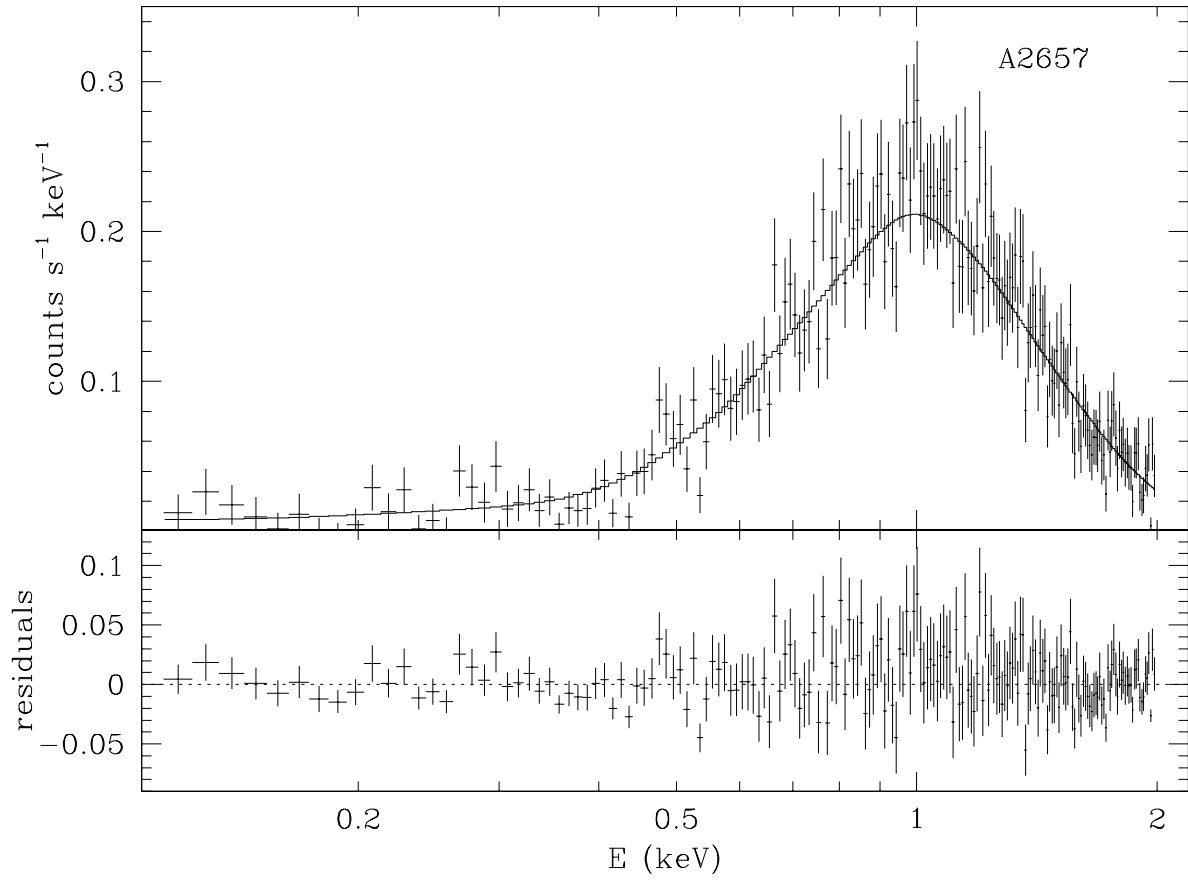


Fig. 2.— Model spectrum of Abell 2657. The model used is a single thermal plasma emission component with intervening absorption set to the Galactic N_x value from AB. The fit is acceptable ($\chi_r^2 = 1.168$).

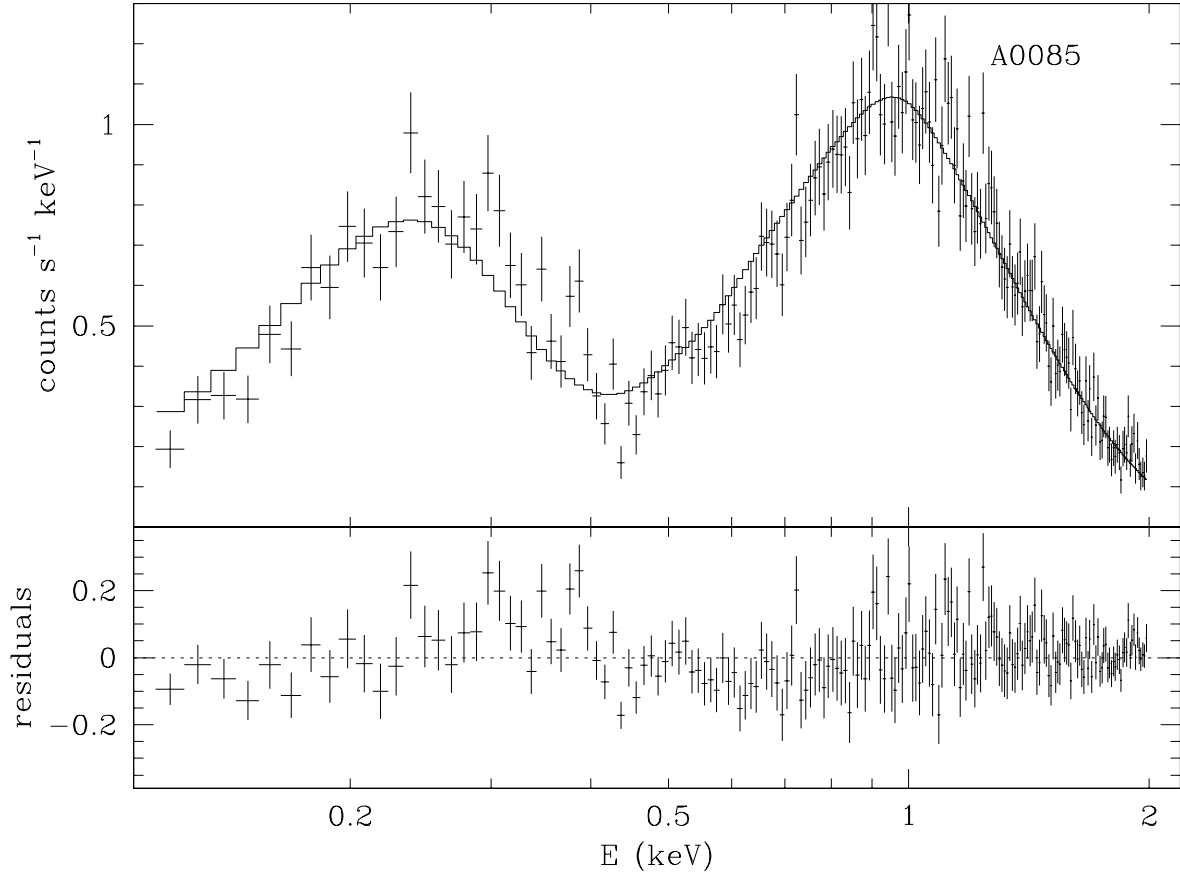


Fig. 3.— Model spectrum of Abell 85. The model used is a two-component thermal plasma with a variable absorption column. In this case the column assumed a value 6% higher than the Galactic value. The fit is marginally unacceptable ($\chi_r^2 > 1.26$).

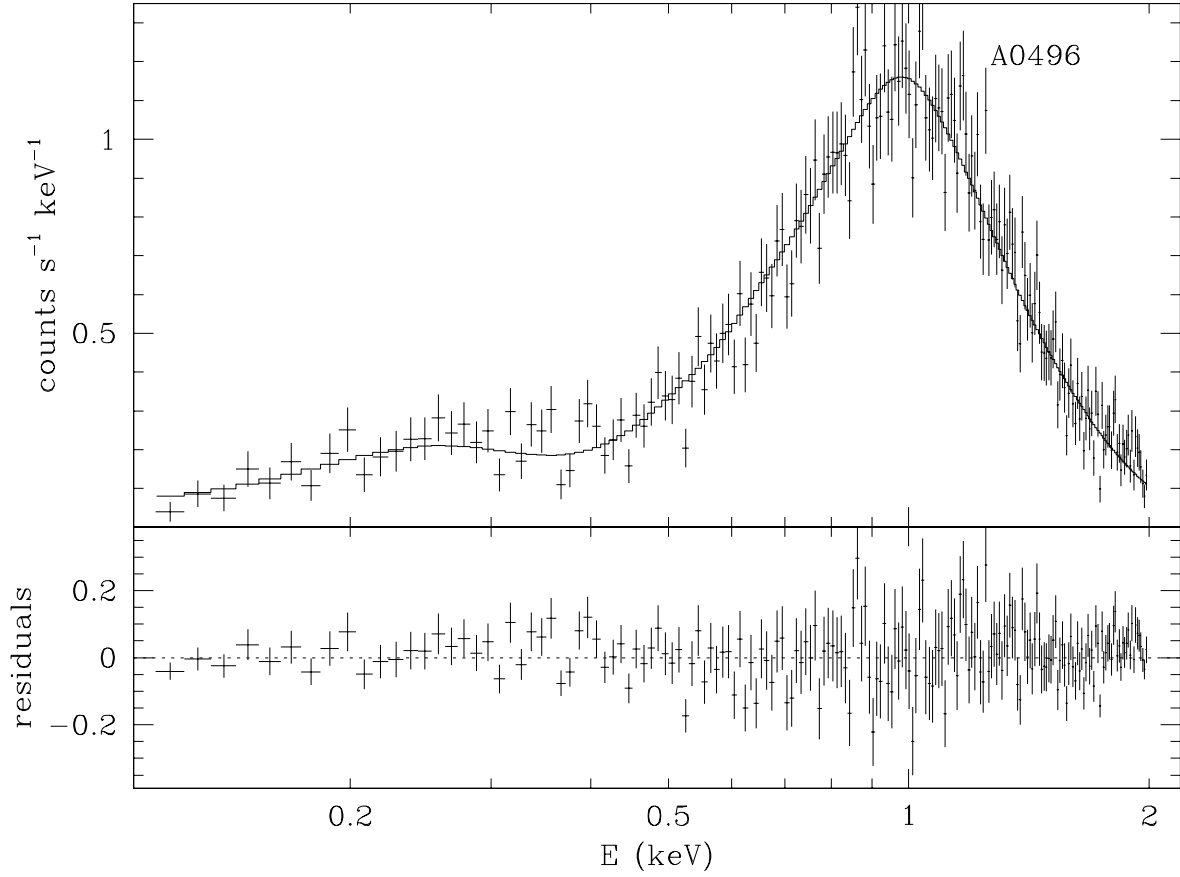


Fig. 4.— Model spectrum of Abell 496. The model used is a two-component thermal plasma with a variable absorption column. Here the column assumed a value 8% lower than the Galactic value. The fit is marginally unacceptable ($\chi_r^2 = 1.27$).

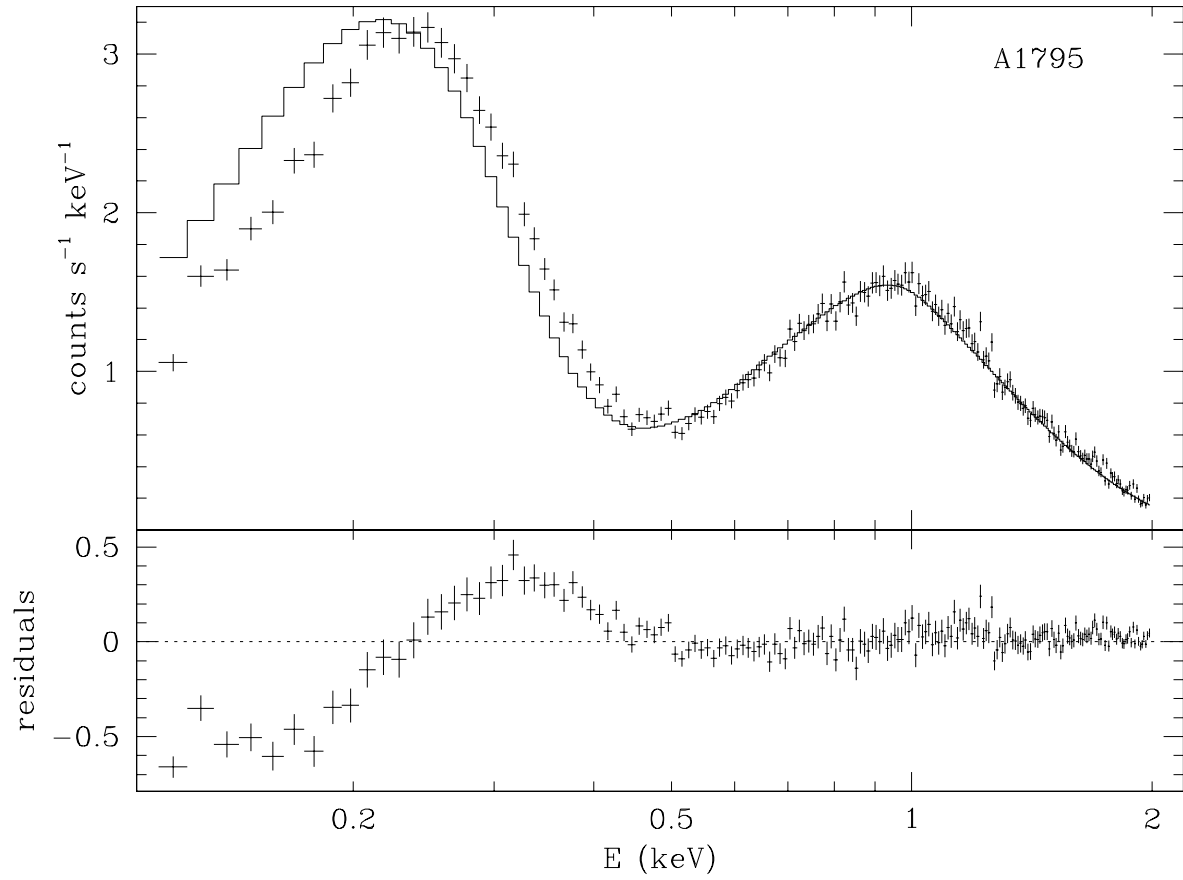


Fig. 5.— Failed two-component model spectrum of A1795. The column here assumed a value 29% above the Galactic value. The systematic errors in the residuals below 0.5 keV are most likely due to a gain offset.

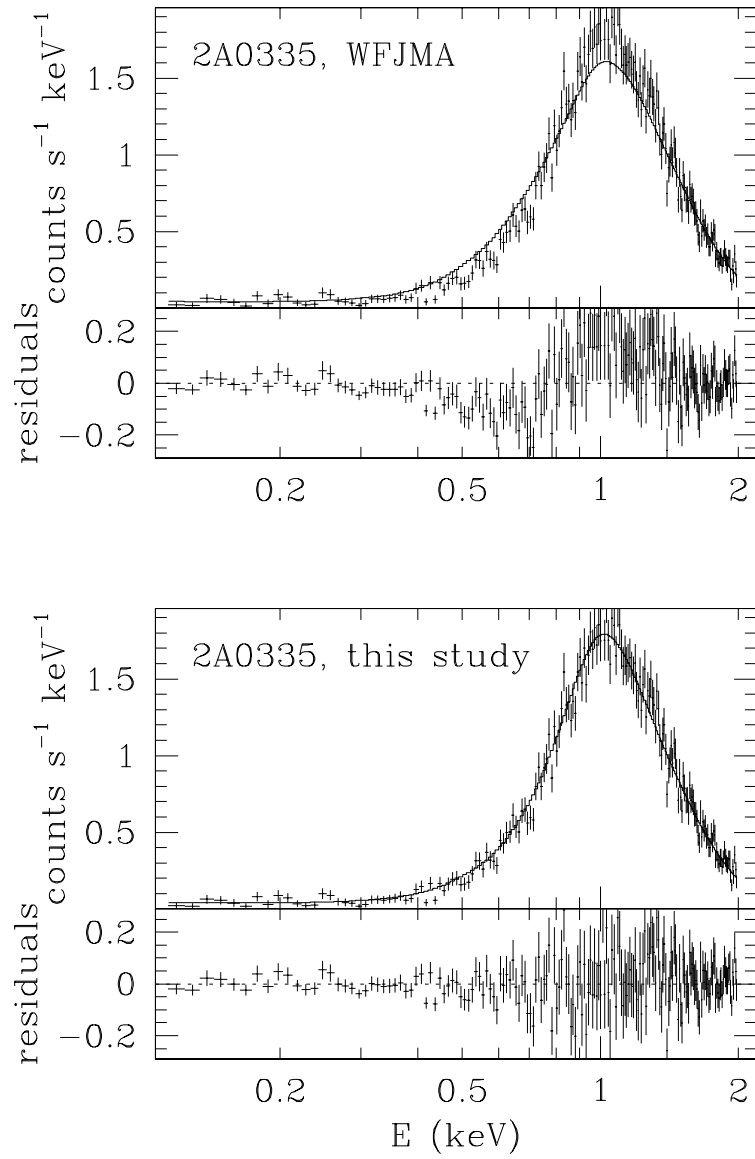


Fig. 6.— A comparison of models for the *ROSAT* spectrum of 2A0335. The top spectrum shows the best-fit WJFMA model applied to the data; the bottom shows the cooling flow and single absorption component model of this study.

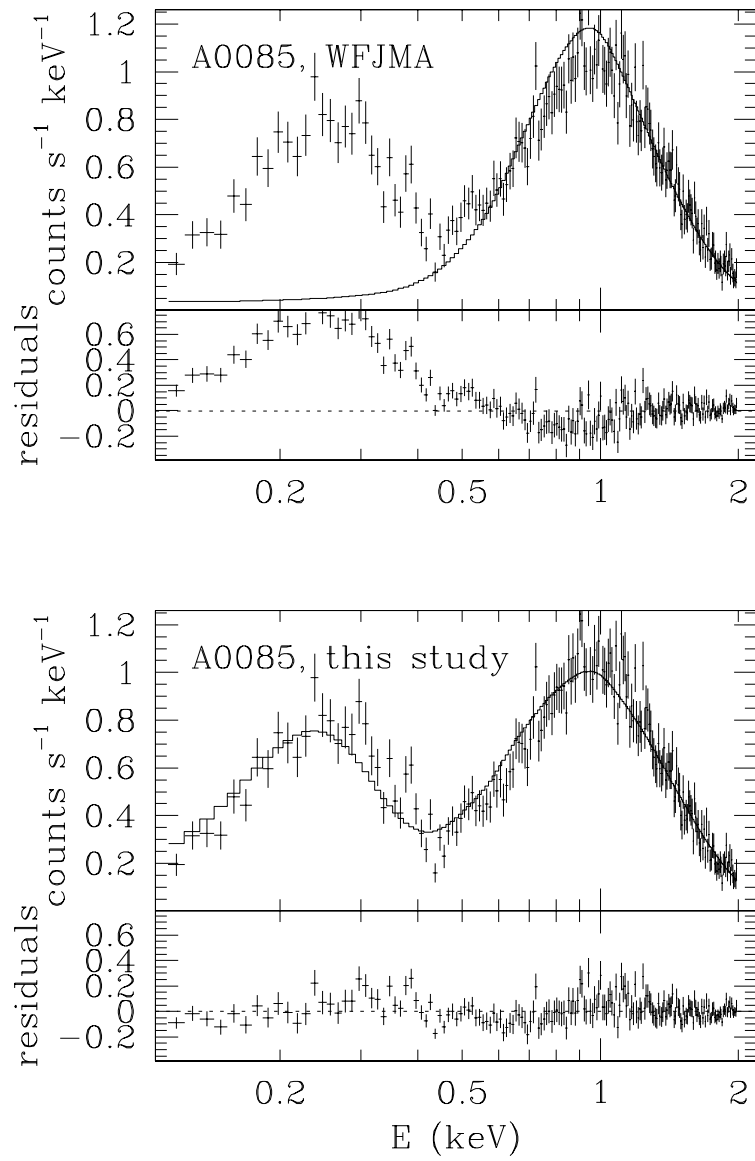


Fig. 7.— A comparison of models for the *ROSAT* spectrum of A0085. The top spectrum shows the best-fit WJFMA model applied to the data; the bottom shows the cooling flow and single absorption component model of this study.

Table 1. The 20 galaxy clusters
in the sample.

cluster	l^I	b^I
2A0335	176.25	–35.08
A0085	115.05	–72.08
A0119	125.75	–64.11
A0133	149.09	–84.09
A0401	164.18	–38.87
A0478	182.43	–28.29
A0496	209.59	–36.49
A0665	149.73	+34.67
A1060	269.63	+26.51
A1651	306.83	+58.62
A1656	58.16	+88.01
A1795	33.81	+77.18
A2029	6.49	+50.55
A2052	9.42	+50.12
A2142	44.23	+48.69
A2147	28.83	+44.50
A2163	6.75	+30.52
A2199	62.93	+43.69
A2256	111.10	+31.74
A2657	96.65	–50.30

Table 2. Model fits to the cluster sample.

cluster	$N_G^{[a]}$	$N_{cf}^{[b,c]}$	$Z^{[d]}$	$T_1^{[e]}$	$e_2^{[f]}$	$T_2^{[g,c]}$	$\dot{M}^{[h]}$	$\chi_r^2^{[i]}$
2A0335	26.1	—	0.5	3.1	–	—	—	2.292
	26.1	—	0.5	3.1	tp	1.70 ± 0.26	—	1.108
	26.1	—	0.5	3.1	cf	$0.08 \pm \infty$	143 ± 15	1.728
	38.6 ± 4.1	—	0.5	3.1	cf	0.35 ± 0.01	574 ± 86	1.250
	26.1	3.3 ± 1.9	0.5	3.1	cf	0.90 ± 0.37	459 ± 64	1.114
A0085	2.79	—	0.5	6.2	–	—	—	1.469
	2.79	—	0.5	6.2	tp	1.40 ± 0.25	—	1.333
	2.96 ± 0.11	—	0.5	6.2	tp	1.57 ± 0.50	—	1.307
	2.79	—	0.5	6.2	cf	$0.08 \pm \infty$	20 ± 13	1.462
	2.97 ± 0.07	—	0.5	6.2	cf	0.36 ± 6.27	14 ± 30	1.427
	2.79	24.2 ± 11.6	0.5	6.2	cf	$0.08 \pm \infty$	43 ± 14	1.375
A0119	3.10	—	0.5	5.1	–	—	—	0.987
	3.10	—	0.5	5.1	cf	$0.08 \pm \infty$	0 ± 3	0.994
	3.41 ± 0.35	—	0.5	5.1	cf	0.35 ± 2.80	5 ± 5	1.026
	3.10	$246 \pm \infty$	0.5	5.1	cf	$0.09 \pm \infty$	0 ± 4	1.000
A0133	1.46	—	0.5	3.8	–	—	—	2.056
	1.46	—	0.5	3.8	tp	1.41 ± 0.14	—	1.625
	1.73 ± 0.09	—	0.5	3.8	tp	1.87 ± 0.40	—	1.499
	1.46	—	0.5	3.8	cf	$0.08 \pm \infty$	0 ± 10	2.078
	1.51 ± 0.06	—	0.5	3.8	cf	1.14 ± 0.02	164 ± 61	1.514
	1.46	$94.4 \pm \infty$	0.5	3.8	cf	$0.09 \pm \infty$	0 ± 10	2.089
A0401	12.6	—	0.3	7.8	–	—	—	1.014
	12.6	—	0.3	7.8	cf	$0.08 \pm \infty$	77 ± 23	1.014
	15.9 ± 0.1	—	0.3	7.8	cf	$0.08 \pm \infty$	102 ± 92	0.973
	12.6	7.1 ± 10.4	0.3	7.8	cf	$0.08 \pm \infty$	108 ± 107	0.982
A0478	37.4	—	0.5	6.8	–	—	—	1.528

Table 2—Continued

cluster	$N_G^{[a]}$	$N_{cf}^{[b,c]}$	$Z^{[d]}$	$T_1^{[e]}$	$e_2^{[f]}$	$T_2^{[g,c]}$	$\dot{M}^{[h]}$	$\chi_r^2^{[i]}$
	37.4	—	0.5	6.8	tp	1.99 ± 0.93	—	1.153
	37.4	—	0.5	6.8	cf	0.35 ± 0.01	620 ± 106	1.223
	40.5 ± 2.3	—	0.5	6.8	cf	0.35 ± 0.97	882 ± 178	1.155
	37.4	12.0 ± 4.1	0.5	6.8	cf	$0.08 \pm \infty$	1197 ± 421	1.134
A0496	7.02	—	0.5	4.7	—	—	—	1.729
	7.02	—	0.5	4.7	tp	1.83 ± 0.30	—	1.300
	6.43 ± 0.23	—	0.5	4.7	tp	1.58 ± 0.30	—	1.273
	7.02	—	0.5	4.7	cf	0.17 ± 0.02	34 ± 7	1.561
	6.57 ± 0.22	—	0.5	4.7	cf	0.17 ± 1.27	34 ± 8	1.538
	7.02	0.0 ± 0.0	0.5	4.7	cf	0.35 ± 0.01	44 ± 11	1.534
A0665	4.73	—	0.5	8.3	—	—	—	1.025
	4.73	—	0.5	8.3	cf	$0.08 \pm \infty$	99 ± 47	1.018
	4.88 ± 0.16	—	0.5	8.3	cf	0.22 ± 4.5	100 ± 96	1.018
	4.73	1.37 ± 23.8	0.5	8.3	cf	0.08 ± 6.8	97 ± 168	1.017
A1060	6.53	—	0.3	3.3	—	—	—	0.864
	6.53	—	0.3	3.3	cf	$0.08 \pm \infty$	0 ± 1	0.859
	6.24 ± 0.35	—	0.3	3.3	cf	0.23 ± 3.27	1 ± 1	0.853
	6.53	0.0 ± 0.0	0.3	3.3	cf	$0.10 \pm \infty$	0 ± 0	0.865
A1651	1.59	—	0.5	7.0	—	—	—	1.444
	1.59	—	0.5	7.0	tp	1.73 ± 0.47	—	1.411
	1.78 ± 0.15	—	0.5	7.0	tp	3.15 ± 3.62	—	1.388
	1.59	—	0.5	7.0	cf	0.28 ± 3.31	45 ± 49	1.441
	1.59 ± 0.74	—	0.5	7.0	cf	0.28 ± 3.38	45 ± 49	1.448
	1.59	$0.02 \pm \infty$	0.5	7.0	cf	$0.22 \pm \infty$	0 ± 25	1.467
A1656	0.597	—	0.3	8.0	—	—	—	1.136
	0.597	—	0.3	8.0	cf	$1.02 \pm \infty$	0 ± 1	1.148

Table 2—Continued

cluster	$N_G^{[a]}$	$N_{cf}^{[b,c]}$	$Z^{[d]}$	$T_1^{[e]}$	$e_2^{[f]}$	$T_2^{[g,c]}$	$\dot{M}^{[h]}$	$\chi_r^2^{[i]}$
	0.587 ± 0.071	—	0.3	8.0	cf	$0.41 \pm \infty$	0 ± 1	1.154
	0.597	0.0 ± 0.0	0.3	8.0	cf	$1.13 \pm \infty$	0 ± 2	1.156
A1795	0.909	—	0.5	5.1	–	—	—	4.886
	0.909	—	0.5	5.1	tp	1.16 ± 0.10	—	5.106
	1.17 ± 0.03	—	0.5	5.1	tp	2.98 ± 0.94	—	3.848
	0.909	—	0.5	5.1	cf	0.56 ± 2.04	83 ± 42	4.501
	1.08 ± 0.02	—	0.5	5.1	cf	1.14 ± 2.64	32 ± 31	3.848
	0.909	$58.8 \pm \infty$	0.5	5.1	cf	$0.11 \pm \infty$	0 ± 21	5.807
A2029	3.23	—	0.5	7.8	–	—	—	2.009
	3.23	—	0.5	7.8	tp	1.29 ± 0.15	—	1.592
	3.59 ± 0.09	—	0.5	7.8	tp	1.29 ± 0.15	—	1.503
	3.23	—	0.5	7.8	cf	0.08 ± 6.97	132 ± 31	1.911
	3.43 ± 0.08	—	0.5	7.8	cf	0.14 ± 2.88	136 ± 33	1.808
	3.23	$4.02 \pm \infty$	0.5	7.8	cf	$0.54 \pm \infty$	0 ± 74	2.041
A2052	3.10	—	0.5	3.4	–	—	—	1.613
	3.10	—	0.5	3.4	tp	1.72 ± 0.23	—	1.215
	3.10	—	0.5	3.4	cf	0.55 ± 5.26	23 ± 33	1.531
	3.08 ± 0.11	—	0.5	3.4	cf	0.71 ± 2.68	24 ± 15	1.525
	3.10	0.0 ± 0.0	0.5	3.4	cf	0.90 ± 0.01	70 ± 31	1.424
A2142	4.17	—	0.5	11.0	tp	—	—	1.283
	4.17	—	0.5	11.0	tp	0.08 ± 0.13	—	1.179
	4.17	—	0.5	11.0	cf	0.08 ± 7.41	188 ± 43	1.190
	4.45 ± 0.17	—	0.5	11.0	cf	0.15 ± 3.46	192 ± 46	1.149
	4.17	1.17 ± 5.87	0.5	11.0	cf	$0.08 \pm \infty$	210 ± 110	1.152
A2147	2.56	—	0.3	4.4	–	—	—	0.497
	2.56	—	0.3	4.4	cf	0.15 ± 4.68	27 ± 12	0.467

Table 2—Continued

cluster	$N_G^{[a]}$	$N_{cf}^{[b,c]}$	$Z^{[d]}$	$T_1^{[e]}$	$e_2^{[f]}$	$T_2^{[g,c]}$	$\dot{M}^{[h]}$	$\chi_r^2^{[i]}$
	2.83 ± 1.06	—	0.3	4.4	cf	0.28 ± 2.43	28 ± 23	0.473
	2.56	0.00 ± 0.03	0.3	4.4	cf	0.22 ± 0.03	24 ± 15	0.638
A2163	26.4	—	0.3	13.9	–	—	—	1.312
	26.4	—	0.3	13.9	tp	2.17 ± 1.60	—	1.124
	26.4	—	0.3	13.9	cf	$0.08 \pm \infty$	1570 ± 278	1.137
	26.7 ± 0.07	—	0.3	13.9	cf	0.35 ± 3.03	1631 ± 874	1.139
	26.4	1.65 ± 10.5	0.3	13.9	cf	$0.08 \pm \infty$	1759 ± 1297	1.139
A2199	0.877	—	0.5	4.7	–	—	—	6.661
	0.877	—	0.5	4.7	tp	1.27 ± 0.05	—	3.992
	1.21 ± 0.03	—	0.5	4.7	tp	1.96 ± 0.16	—	2.770
	0.877	—	0.5	4.7	cf	0.09 ± 0.84	24 ± 2	5.300
	1.03 ± 0.02	—	0.5	4.7	cf	0.35 ± 0.01	26 ± 3	4.280
	0.877	2.34 ± 1.27	0.5	4.7	cf	0.17 ± 1.02	14 ± 2	4.705
A2256	4.65	—	0.3	7.5	–	—	—	1.367
	4.65	—	0.3	7.5	tp	0.86 ± 0.18	—	1.294
	4.52 ± 0.19	—	0.3	7.5	tp	0.87 ± 0.19	—	1.298
	4.65	—	0.3	7.5	cf	0.08 ± 9.44	14 ± 6	1.307
	4.46 ± 2.61	—	0.3	7.5	cf	$0.08 \pm \infty$	21 ± 11	1.293
	4.65	0.0 ± 0.0	0.3	7.5	cf	0.08 ± 0.22	15 ± 6	1.311
A2657	11.3	—	0.5	3.4	–	—	—	1.168
	11.3	—	0.5	3.4	cf	0.90 ± 1.12	17 ± 8	1.138
	12.6 ± 1.5	—	0.5	3.4	cf	0.71 ± 2.07	29 ± 15	1.077
	11.3	13.4 ± 11.1	0.5	3.4	cf	$0.08 \pm \infty$	35 ± 31	1.073

^[a]Intervening Galactic hydrogen column density in units of 10^{20} cm^{-2} .

^[b]Column density of separate cooling flow absorption component in units of 10^{20} cm^{-2} .

^[c] ∞ indicates that the error in the quantity exceeds the quantity by a factor of >100 .

^[d]Metallicity of emission component(s).

^[e]Temperature of emission component 1 (keV).

^[f]Emission component 2: tp = thermal plasma; cf = cooling flow; – = none.

^[g]Temperature of emission component 2 for the thermal plasma, or low-temperature cut-off of the cooling flow (keV).

Table 3. Excess absorption, internal absorption, and cooling rates in cluster models.

cluster	$\Delta N_x/N_G$	$\Delta N_x/N_G$	$\Delta N_x/N_G$	N_{cf}/N_G	\dot{M}	\dot{M}	\dot{M}
	WFJMA	tp + tp	tp + cf	tp + acf	WFJMA	tp + cf	tp + acf
	% ^a	% ^b	% ^c	% ^d	M_\odot/y ^e	M_\odot/y ^f	M_\odot/y ^g
2A0335	$+90 \pm \frac{30}{30}$	0	$+48 \pm 16$	13 ± 7	$105 \pm \frac{88}{66}$	574 ± 86	459 ± 64
A0085	$+330 \pm \frac{170}{130}$	$+6 \pm 4$	$+6 \pm 3$	867 ± 414	$290 \pm \frac{138}{130}$	14 ± 30	43 ± 14
A0401	$+190 \pm \frac{110}{70}$	0	$+26 \pm 1$	56 ± 83	$111 \pm \frac{236}{111}$	102 ± 92	108 ± 107
A0478	$+300 \pm \frac{60}{50}$	0	$+8 \pm 6$	32 ± 11	$495 \pm \frac{580}{424}$	882 ± 178	1197 ± 421
A0496	$+470 \pm \frac{90}{60}$	-8 ± 3	-6 ± 3	0 ± 0	$65 \pm \frac{29}{23}$	34 ± 8	44 ± 11
A1656	$-100 \pm \frac{670}{0}$	0	-2 ± 12	0 ± 0	$16 \pm \frac{29}{15}$	0 ± 1	0 ± 2
A1795	$+730 \pm \frac{270}{270}$	$+29 \pm 3$	$+19 \pm 2$	647 ± 2700	$225 \pm \frac{144}{112}$	32 ± 31	0 ± 21
A2029	$+580 \pm \frac{160}{160}$	$+11 \pm 3$	$+6 \pm 2$	124 ± 6900	$513 \pm \frac{304}{247}$	136 ± 33	0 ± 74
A2142	$+340 \pm \frac{80}{110}$	0	$+7 \pm 4$	28 ± 141	$143 \pm \frac{141}{130}$	192 ± 46	210 ± 110
A2147	$+330 \pm \frac{210}{180}$	0	$+10 \pm 41$	0 ± 114	$28 \pm \frac{25}{12}$	28 ± 23	24 ± 15
A2199	$+1560 \pm \frac{220}{200}$	$+38 \pm 3$	$+17 \pm 2$	267 ± 145	$60 \pm \frac{20}{17}$	26 ± 3	14 ± 2
A2256	$-100 \pm \frac{240}{20}$	-3 ± 4	-4 ± 56	0 ± 0	$200 \pm \frac{140}{90}$	21 ± 11	16 ± 6

^a Change in the X-ray absorption column when it is allowed to deviate from $N_{21\text{cm}}$ taken from Stark et al. (1992).

^b Change in the X-ray absorption column when it is allowed to deviate from N_x taken from AB. The emission is modelled as a one- or two-component thermal plasma. A zero indicates that an acceptable fit was obtained by setting the absorption to the Galactic column from AB.

^c Change in the Galactic X-ray absorption column when it is allowed to deviate from N_x taken from AB. The emission is modelled as a thermal plasma plus a cooling flow, with the absorption column a free parameter.

^d Absorption column of a separate absorption component (relative to the Galactic column) which covers only the cooling flow.

^e Mass deposition rate in the WFJMA cooling flow.

^f Mass deposition rate in the cooling flow models of this study with variable Galactic absorption.

^g Mass deposition rate in the cooling flow models of this study with variable cluster cooling flow absorption.